# Reducing power peaks in railway traffic flow subject to random effects

Alessio Trivella[a,*], Francesco Corman[b]

[b]Industrial Engineering and Business Information Systems, University of Twente, 7500 AE Enschede, The Netherlands

[a]Institute for Transport Planning and Systems, ETH Zürich, 8092 Zürich, Switzerland

Railway traffic flow in a corridor can be modeled by a string of consecutive trains, each subject to random speed variations that are described by a stochastic process. Despite analogies with car-follower models, railways include specific features and a safety system that forces vehicles to decelerate towards a fixed lower speed if an absolute safety distance with the vehicle ahead is not respected. We simulate such a dynamic system under assumptions that model human drivers and automated train operations (ATO), and compute performance measures focusing on energy consumption and the power peaks arising when multiple trains accelerate simultaneously. We investigate measures to smooth these peaks including the use of regenerative braking energy, potentially coupled with an electric energy storage, and a rule that uses fixed waiting times before re-accelerating. Our findings shed light on when and why these measures can be effective at reducing energy consumption and/or shaving the peaks, and show that employing a well-calibrated ATO controller improves energy performance compared to a model of a human driven. Our results also expose a trade-off between the energy performance and the regularity of the traffic, i.e., strategies to reduce power peaks may slow rail traffic down, leading to a lower capacity utilization.

KEYWORDS: Railway traffic dynamics; stochastic processes; traffic flow theory; power peaks; automated train operations.

## 1. Introduction

Transport accounts for a large share of energy consumption and is responsible for about 16% of greenhouse gas emissions globally (OWiD 2016). Since three quarters of this amount is attributed to road transport, one key direction to promote sustainability and energy efficiency is to switch to collective transport of larger vehicles, rather than using private vehicles or small shipments by trucks. Railway is generally acknowledged to be an energy-efficient mode of transporting passenger and freight. Nonetheless, efforts to reduce its energy footprint are pursued by many transport operators and authorities (UIC 2017) to cope with skyrocketing energy prices and to meet ambitious climate targets, e.g., set by the European Union for 2030 (EU 2021).

In fact, energy consumption accounts for a large portion of railway operations costs (Railenergy 2016). The amount of energy needed for moving a train depends on speed and resistances, and

*Corresponding author. E-mail: alessio.trivella@utwente.nl

results in requirements for energy production. By carefully planning the acceleration and braking processes of trains (i.e., the so-called train speed profiles) or optimizing the timetable, significant energy can be saved (Hansen and Pachl 2014). In electrified railway systems, energy usage is centralized, i.e., all vehicles draw energy at the same time from a distribution network. The total energy required by the system is then the sum of all energies required by all vehicles. Nowadays, many rail electric systems can exploit regenerative braking, i.e., the motor of a decelerating train is turned to a generator that converts mechanical energy to electricity, which can be then used to power nearby trains (Lu et al. 2014, Khodaparastan et al. 2019), potentially in conjunction with an energy storage (González-Gil et al. 2013, De La Torre et al. 2014).

In addition to energy consumption, it is important to consider the peak value of the power needed. Power peaks arise when multiple vehicles require large amount of power, for instance during acceleration. Those peaks threaten grid stability and represent a big concern for operators (Wang et al. 2022). A power distribution network designed for lower peaks might fail when the power demand is very high, causing reduction of delivered energy or, in the worst cases, a blackout. Traffic volume is growing, speed is increasing, vehicles are heavier, resulting in higher chances of high power peaks, but redesigning or upgrading the power distribution requires large costs and long time. Overdimensioning the power network at the design stage is also very costly. In addition to grid stability, another issue with power peaks is that the energy bill paid by rail operators is usually based on both total and maximum consumption (i.e., the highest peak) over the billing period (Albrecht 2010). Smoothing power peaks has thus a direct impact on operational costs.

Controlling the total and maximum energy consumption of a railway system is challenging because practical railway operations are unavoidably subject to uncertainties affecting running and waiting times of trains. Even though accounting for energy consumption when designing the train timetable is common (Yang et al. 2015), disturbances occurring in real time shift departure and arrival times of trains and alter the planned timetable and synchronization of acceleration activities. At a microscopic level, a train is subject to random speed variations that are linked with the driver behaviors and changes in line voltage and track resistance, among others. Corman et al. (2021) provides empirical evidence of this effect using data from the Swiss railway, and introduces stochastic processes to model a system with two trains. The dynamic characteristics of a follower train are studied given a trajectory of a leader, without looking at energy use.

In this paper, we study a stochastic model of railway traffic flow for a more generic string of $N$ consecutive trains. As opposed to car traffic, railway vehicles are subject to a strict safety system and must keep a minimum safety distance. When two trains get too close, a yellow signal is triggered and the follower must decelerate towards a fixed lower speed. This results in extra time lost, in a braking, and a successive re-acceleration to a cruising speed. When multiple consecutive trains are considered, a yellow signal may cause a cascade effect on downstream vehicles, forcing more trains to decelerate and re-accelerate, possibly producing a power peak. We are thus particularly

interested in examining this behavior for a string of trains, its implications, and possible strategies to improve traffic regularity, energy usage, and peak values.

We consider three models to describe railway traffic dynamics, namely a deterministic baseline and two stochastic models describing, respectively, a human driver and an automated train operations (ATO) controller. We also consider different strategies to reduce the peaks based on technological assumptions and/or train control. One strategy implements fixed waiting rules for trains that have triggered a yellow signal. Another measure assumes that the electric railway system can use regenerative braking energy, possibly combined with an electric energy storage. We use simulation for each model and strategy to quantify the emerging properties of the system, with focus on energy consumption and power peaks. Our simulation program is coded in Matlab and is made available online[1].

The key takeaways from our work are the following:

- The model describing an ATO controller is more efficient than that of a human driver in terms of traffic regularity, consumes less energy, and results in fewer power peaks.
- The considered strategies can shave the power peaks quite effectively. Under the human driver model, for instance, accounting for regenerative braking lowers the overall energy consumption by 3.3%, while coupling this with a storage reduces the peak height by 10%. Combining all strategies further decreases consumption and peaks.
- There is a trade-off between traffic regularity (measured, e.g., as the throughput, i.e., the hourly number of vehicles crossing the corridor) and energy performance (intended as energy consumption and power peaks). Strategies to improve energy performance must be designed and tuned carefully to avoid significant losses in capacity utilization.

In the following, we review relevant literature in Section 2, introduce the methodology in Section 3, present and discuss numerical results in Section 4, and conclude in Section 5.

## 2. Novelty and related work

We review three main streams of literature connected with our research: improving energy efficiency in railway operations (Section 2.1), dealing with stochasticity in railway models (Section 2.2), and traffic flow theory (Section 2.3). We then summarize the contributions of our study (Section 2.4).

### 2.1 Energy efficiency in railways operations

There is a considerable body of literature dealing with the energy efficiency of railway systems (De Martinis and Corman 2018). Two prominent ways to cut energy consumption at the operational level (i.e., without costly investments in new vehicles or electric systems) involve optimizing the train speed profiles and the timetable.

[1] https://alessiotrivella.altervista.org/research.htm

Computing an energy-efficient speed profile for a train running between two stations is commonly known as the train trajectory optimization problem or the energy-efficient train control problem. Here, a speed profile describes the speed of a train as a function of time or distance covered. Determining such a profile means choosing the driving regimes (acceleration, cruising, coasting, and deceleration) and the switching points between them (Howlett 2000). The goal is finding the profile associated with the lowest energy use, while ensuring a punctual arrival and respecting speed limits and time windows. It is well known that optimizing train control can lead to large energy savings, also above 10% (Hansen and Pachl 2014). Methods to tackle this problem include the Pontryagin's maximum principle (Albrecht et al. 2016), mathematical programming (Ye and Liu 2017), and dynamic programming (Trivella et al. 2021). Since we consider a stochastic dynamic system comprised of multiple trains, our problem deviates from the train trajectory optimization problem, although both problems deal with speed variations and train control at a microscopic scale.

The timetabling problem aims at determining departure and arrival times of trains at stations subject to headway and track capacity constraints (Caprara et al. 2002). The traditional objectives are to minimize operational costs (e.g., number of required vehicles), maximize passenger satisfaction (e.g., by reducing travel time), and minimize deviations from the original timetable in case of a disruption (Binder et al. 2017). Recently, emphasis has been put on the energy use associated with a timetable. Bärmann et al. (2017) discusses how minimal changes in the planned timetables can impact energy and power of the entire system. Regueiro Sánchez (2021) adopts a similar approach, also limiting the maximum traction power available between stations. Wang et al. (2022) tunes a timetable using a mixed-integer linear program combined with a local search algorithm, with the goal of reducing energy consumption and smoothing power peaks.

We refer to the review by Scheepmaker et al. (2017) for further literature on both the energy-efficient train control and the energy-efficient train timetabling. Some works attempted to combine these two problems by embedding train control between pairs of stations as a subproblem into a timetable optimization framework (Yang et al. 2015, Ran et al. 2020). Although our work also considers a system of interacting trains, the problem we tackle is quite different than timetabling as we focus on a string of trains running in a corridor; hence, we are not concerned with setting departure and arrival times.

Finally, in addition to designing the timetable, real-time train rescheduling models are used to modify the planned timetable and avoid conflicts when disturbances or disruptions occur. The related literature prioritizes recovering the delays over reducing energy use. An exception is Yin et al. (2016) that includes energy considerations when rescheduling a metro system.

## 2.2 Stochasticity in railway models

The majority of the aforementioned works assume that the future is known with certainty at the planning stage. However, railway operations are characterized by uncontrollable stochastic factors that only realize in real time. Those include variable passenger demand, boarding/alighting times, running times, technical failures, and weather to name a few (Trivella and Corman 2019).

Some recent literature has acknowledged that accounting for uncertainty and counteracting it is critical. Thus, uncertainty has been incorporated into train control, timetabling, and rescheduling models (Yin et al. 2016, Yang et al. 2016, Wang et al. 2020, Cacchiani and Toth 2018, Jusup et al. 2021). For instance, the goal of (Cacchiani and Toth 2018) is to compute train timetables that are robust, i.e., that are expected to perform well under random disturbances. Wang et al. (2020) uses approximate dynamic programming to tackle train control in the case of randomly varying speed profiles due to uncertain resistance parameters. Yin et al. (2016) uses similar methods to reschedule a metro network under uncertain passenger demands. Yang et al. (2016) proposes an integrated stochastic model for optimizing speed profile and timetable in metro systems under uncertain train mass.

In our paper, we consider random variations affecting train speed at the microscopic level. While most approaches capture the uncertainty dynamics by simple independent and identically distributed random variables, we model the uncertainty in train speed by a stochastic process. It refers to a collection of random variables that are function of time, and where the outcome of the process at a time $t$ also depends on its value at time $t-1$. These are more sophisticated models that were shown to describe well real-life situations (Corman et al. 2021). When considering a string of trains, the complexity increases and it is not possible to derive closed-form expressions using the stochastic differential equations governing the processes. Therefore, we can only rely on simulation to study the system dynamics, and derive the relevant performance measures as sample averages over a large number of Monte Carlo sampled trajectories.

## 2.3 Traffic flow theory

This work builds on the stochastic modeling of railway operations, which extends the vehicular traffic flow theory to railway systems (Corman et al. 2021). Whilst Corman et al. (2021) focuses on a system of two trains (on which only one subject to random effects) and on the regularity of the traffic, we consider in this paper a system of $N$ trains, and examine its behavior in terms of energy consumption and power peaks. Apart from this reference, the literature on traffic flow theory has almost exclusively tackled car traffic, which has similarities with our study but also important differences.

In the case of private vehicles, there is no external safety system which constrains their speeds and distances in-between, which is instead a key feature of railways. When vehicles can be individually controlled, an interesting problem of traffic flow theory is to study under which conditions, a series of

successive coordinated vehicles has impact towards traffic flow stability, i.e., studying string stability. This has been mostly focusing on vehicles with homogeneous, simplified characteristics (Wang et al. 2017). A second difference is that power distribution in railway traffic is pooled and centralized; hence, there exist issues with simultaneous high energy maneuvers of different vehicles. In contrast, studies of vehicular traffic do not focus on power peaks because the energy consumption of all vehicles draws from separated energy carriers (such as internal combustion engines, or battery-fed electric motors), although this may change should electric highway systems become more popular in the future. Nevertheless, there is interest in minimizing system properties such as emissions (Qin et al. 2020, Zhang et al. 2020), which have some of their sources in speed and acceleration.

### 2.4 Summary of contribution

This work contributes to the literature by drawing a bridge between the three different active fields of research previously reviewed. The main contribution of this paper is threefold:

- We extend existing two-train stochastic process models by simulating and studying the behavior of a string of multiple consecutive trains, with focus on energy use;
- We outline a technique for detecting the power peaks arising in the resulting dynamic system, and propose three strategies to smooth such peaks based, e.g., on train control and/or managing an energy storage;
- We provide insights on the impact of different processes (e.g., modeling a human driver vs ATO) and different peak reduction strategies towards traffic regularity, energy use, power peaks, and the trade-offs between these goals.

## 3. Methodology

We first present in 3.1 the two stochastic process models for a string of trains and the deterministic benchmark. We then introduce the performance indicators of interest in 3.2, and how to obtain them via simulation. We outline our method for detecting peaks in energy consumption in 3.3, and finally describe different strategies to smooth these peaks in 4.4.

### 3.1 Stochastic models of railway traffic flow

Following the model for two trains in Corman et al. (2021), we define a general stochastic system of $N$ consecutive trains that are initially spaced at a safe distance one from another. Denote by $v_n(t)$ and $s_n(t)$, respectively, the speed and distance covered by train $n$ at time $t \geqslant 0$. Also denote by $W(t)$ a standard Wiener process and by $v_{\text{CRUISE}}$ a reference cruising speed for all trains. The first model we consider is based on the Ornstein-Uhlenbeck (OU) stochastic process, expressed for train $n$ as:

$$[\text{OU}]: \begin{cases} \mathrm{d}v_n(t) = \beta_n(v_{\text{CRUISE}} - v_n(t))\mathrm{d}t + \sigma_n \mathrm{d}W(t), \\ \mathrm{d}s_n(t) = v_n(t)\mathrm{d}t. \end{cases} \tag{1}$$

with boundary conditions $v_n(0) = v_{\text{CRUISE}}$ and $s_n(0) = 0$, i.e., all trains are already running at time 0. The stochastic differential equation (1) describes the microscopic variations of speed and space over time. Based on this equation, the train speed varies according to a deterministic component that establishes the mean reverting behavior towards $v_{\text{CRUISE}}$, and a stochastic component. At a high level, this model can describe a human train driver that continuously adjusts the train speed to keep it as close as possible to the target value. The parameters defining mean reversion ($\beta_n$) and volatility ($\sigma_n$) capture the reaction of the driver and of the speed control system.

A more sophisticated model is based on a doubly-mean-reverting (DMR) process, describing an ATO system where trains are aware of the location of the traffic ahead. Under this model, train $n$ accelerates or decelerates to maintain both a target speed and a target headway with train $n-1$:

$$\text{[DMR]:} \begin{cases} \mathrm{d}v_n(t) = \big[\beta_n(v_{\text{CRUISE}} - v_n(t)) + \alpha_n(s_{n-1}(t) \\ \qquad\qquad -s_n(t))\big]\,\mathrm{d}t + \widehat{\sigma}_n(v_n(t))\,\mathrm{d}W(t), \\ \mathrm{d}s_n(t) = v_n(t)\mathrm{d}t, \end{cases} \tag{2}$$

where $\widehat{\sigma}_n(v) := \sigma_n\sqrt{v(v_{\text{MAX}} - v)/\big[v_{\text{CRUISE}}(v_{\text{MAX}} - v_{\text{CRUISE}})\big]}$, $v_{\text{MAX}} > v_{\text{CRUISE}}$ is an upper bound on speed, and $\alpha_n$ is a second mean reversion parameter that acts on the headway value. We assume the same boundary conditions to model (1) apply. Let us take a closer look at the new term $\alpha_n(s_{n-1}(t) - s_n(t))$. Since $s_n(t)$ represents the distance covered by train $n$ at time $t$, a positive difference $s_{n-1}(t) - s_n(t) > 0$ implies that the preceding train $n-1$ has covered a larger distance than train $n$, hence the headway between the two vehicles has increased. In this case, $\alpha_n(s_{n-1}(t) - s_n(t)) > 0$ will push the speed $v_n(t)$ up, i.e., the current train $n$ accelerates to restore the initial headway. Conversely, with negative distance $s_{n-1}(t) - s_n(t) < 0$, indicating that the headway is shrinking, the stochastic process will steer train $n$ to slow down to restore the headway.

The complete system dynamics couple either (1) or (2) with a deterministic deceleration phase (at a rate $a_{\text{DET}}$) that is triggered when the distance between two trains decreases below a minimum safety distance $d_{\text{MIN}}$, until an approach speed $v_{\text{APPROACH}} < v_{\text{CRUISE}}$ is reached. We assume that at $t = 0$ all trains have a regular headway $d_0 > d_{\text{MIN}}$ from the immediate follower. Notice that the way in which trains interact is a key difference between models (1) and (2). In the former model, the stochastic processes governing each train are independent from each other (trains are only linked by the triggering of yellow signals), whereas in the latter model, the evolution of the state variables for one train (speed, space) also depends on the state variables of the train ahead.

We finally consider a deterministic benchmark that does not account for stochasticity, which is defined by:

$$\text{[DET]:} \begin{cases} \mathrm{d}v_n(t) = 0\mathrm{d}t, \\ \mathrm{d}s_n(t) = v_n(t)\mathrm{d}t. \end{cases} \tag{3}$$

If the deterministic initial speeds are $\bar{v}_n = v_n(0) = v_{\text{CRUISE}}$ for all vehicles $n = 1\ldots, N$, then the

system is in an ideal but unrealistic state in which all train pairs will indefinitely preserve the initial headway. Instead, if the speeds are different and $\bar{v}_n > \bar{v}_{n-1}$ for some $n$, a yellow signal will be triggered at some time $t > 0$ causing train $n$ to decelerate. Once the approach speed is met, this train will then re-accelerate, reaching again $\bar{v}_n > \bar{v}_{n-1}$, trigger a second yellow signal, hence decelerate, and keep cycling over these states. When multiple trains have different initial speeds, the deterministic system will produce much more complex yet cyclic patterns.

### 3.2 Performance indicators and their estimation

We compute key performance indicators (KPIs) of the system related to traffic regularity and energy usage by drawing scenarios (i.e., sample paths) from the stochastic processes in Monte Carlo simulation. We consider an horizon $[0, T]$, discretize it into steps $\mathcal{T} = \{0, 1, \ldots, T\}$ that are equally spaced by $\Delta t$, and apply a standard forward Euler scheme to (1) or (2) to obtain speed and space trajectories, i.e., functions describing the evolution of speed and space of all trains over time.

To derive train acceleration $a_t$, traction force $f_t$, and energy consumption $e_t^n$ at all discrete time steps $\mathcal{T}$, we employ the common dynamic equations for the motion or a railway vehicle[2]. Specifically, the traction force is $f_t = a_t \cdot m \cdot \rho + [\gamma_1 + \gamma_2 v_t + \gamma_3 v_t^2]$,where $a_t = (v_t - v_{t-1})/\Delta t$ is the acceleration, $\gamma_i$ are the train resistance parameters, $m$ the mass, and $\rho$ the rotating mass factor. The energy consumed at time $t$ (with no regenerative braking) is then $e_t^n = \max\{f_t, 0\} \cdot (s_t - s_{t-\Delta t})$. We refer to Hansen and Pachl (2014) for more details on train dynamics.

Using the described simulation procedure, we estimate the six KPIs listed below related to traffic regularity (items 1–3) and energy consumption (items 4–6). Hereafter an *energy profile* $E := \{e_t : t \in \mathcal{T}, e_t = \sum_{n=1}^{N} e_t^n\}$ indicates the joint energy consumption of all trains as a function of time, measured over regular time intervals (e.g., of 30 seconds) during $[0, T]$.

K1. Percentage of scenarios with a triggered yellow signal.

K2. Average first time to yellow (FTTY), which records the first time (s) in which a train triggers a yellow signal (scenarios without signals count as $T$ in the average).

K3. Throughput of the corridor (vehicles/hour) measured as the train speed over headway, where speed and headway are averaged across trains, time steps, and scenarios.

K4. Total energy consumption (kWh) of all $N$ trains over the horizon $[0, T]$, averaged across scenarios.

K5. Maximum value of the energy profile (kWh/30s) over the horizon $[0, T]$, averaged across scenarios.

[2]To ease reading, we drop the dependency on the train index $n$ from $a_t$, $f_t$, $v_t$, *and* $s_t$, and only keep index $n$ for the energy consumption $e_t^n$.

K6. Percentage of energy profiles with a power peak, where a *power peak* is defined as the energy (kWh) consumed during a relatively short period of time that considerably exceeds average consumption levels of the system. The average consumption level refers to the situation where all trains run at cruising speed without disturbances.

Notice that deriving the aforementioned KPIs in closed form using the stochastic differential equations (1)–(2) is not viable for our system. Previous research had already highlighted this challenge: even for the simplest stochastic process and a single train subject to random speed variations, only one KPI (the FTTY) could be computed analytically (Corman et al. 2021).

### 3.3 Power peak detection

Since thousands of simulations are needed to obtain statistically relevant averages, hence reliable KPIs, a method to detect power peaks in a simulated energy profile is needed. Peaks are relative to the railway system considered, e.g., number of trains in the system, their cruising speed, etc. Therefore, we propose to identify them based on a non-parametric procedure that requires no assumptions on the input data and energy profiles.

**Algorithm 1:** Peak detection

**Input:** Energy profile $E = \{e_t : t \in \mathcal{T}\}$; Parameters $(w, \theta_1, \lambda_1, \theta_2, \lambda_2)$, with $\theta_1 \geqslant \theta_2$ and $\lambda_1 \geqslant \lambda_2$; Set of peak points $P \leftarrow \varnothing$; Variable $FullPeakFound \leftarrow FALSE$

**Step 1.** Apply Gaussian filter to $E$ with window $w$ to get a smoothed energy profile $\widehat{E} = \{\widehat{e}_t : t \in \mathcal{T}\}$

**Step 2.** Compute mean ($z$) and standard deviation ($g$) of $\widehat{E}$

**Step 3.** Initialize peak points $P \leftarrow \{t \in \mathcal{T} : \widehat{e}_t \geqslant \theta_1 z + \lambda_1 g\}$

**while** *FullPeakFound* $=$ *FALSE* **do**

  **Step 4.** Try to extend peak points set:
  $P^N \leftarrow \{t \in \mathcal{T} \backslash P : \widehat{e}_t \geqslant \theta_2 z + \lambda_2 g \wedge (\widehat{e}_{t-1} \in P \vee \widehat{e}_{t+1} \in P)\}$

  **if** $P^N = \varnothing$ **then**

    $FullPeakFound \leftarrow TRUE$

  **else**

    $P \leftarrow P \cup P^N$

**Output:** Peak points $P \subset \mathcal{T}$

The method we propose is outlined in Algorithm 1. In a nutshell, we initially define as peaks the points marked as outliers according to a metric based on mean and standard deviation of the overall profile (Steps 2–3). Doing this requires applying first a Gaussian-weighted moving average filter (Step 1) to obtain a smoothed profile, so that we can exclude points with high value due to the background stochastic speed fluctuations. In other words, the effect of this filtering step is to smooth the fluctuations resulting from the stochastic process, while preserving the major peaks that arise when multiple trains accelerate. Finally, we reconstruct the entire peak by iteratively

incorporating neighboring peak points that fulfill a relaxed outlier condition (Step 4).

We show examples of our peak detection procedure for a six-train OU process in Figure 1. We verified that our method is accurate as the identified peaks correspond indeed, in almost all cases, to multiple trains accelerating after a yellow signal.

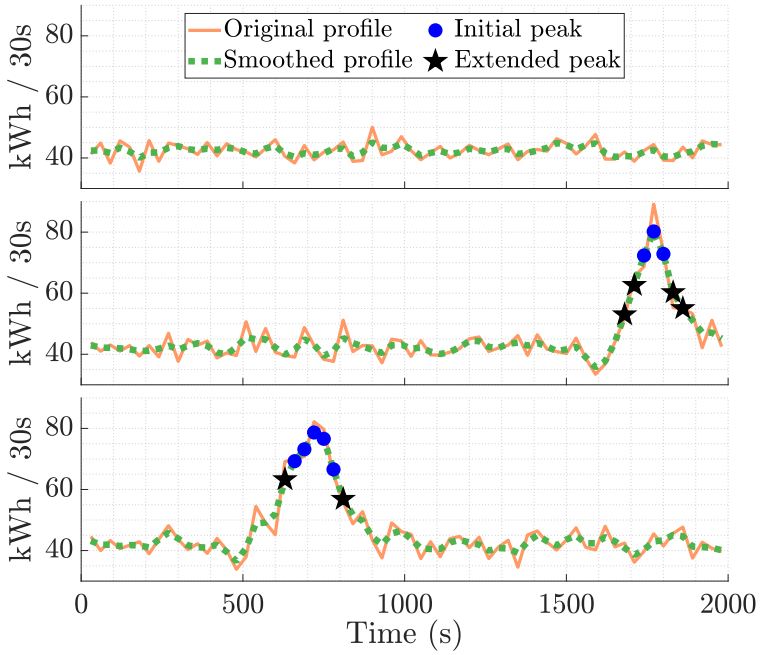


Figure 1: Examples of simulated energy profiles and detected peaks.

### 3.4 Power peak reduction

We study three measures to mitigate the impact of yellow signal propagation: (i) regenerative braking, (ii) managing regenerative energy by means of a storage, and (iii) adopting waiting policies for trains that have triggered a yellow signal. We describe these measures starting with regenerative braking.

Recall that the traction force is computed as $f_t = a_t \cdot m \cdot \rho + [\gamma_1 + \gamma_2 v_t + \gamma_3 v_t^2]$. When a train brakes, $a_t < 0$, which may result in $f_t < 0$. Without regenerative braking, a negative traction force does not contribute to energy use. Regenerative braking allows to convert a portion $\eta \in [0, 1]$ of kinetic energy to electric energy. Mathematically, this means computing

$$e_t^n = \max\{f_t, -\eta f_t\} \cdot (s_t - s_{t-\Delta t}). \tag{4}$$

Thus, the energy recuperated by train $n$ is $r_t^n = |\min\{e_t^n, 0\}|$, and a positive energy $r_t^n > 0$ can only be used by other trains $n' \neq n$ at the current time step $t$. The total regenerative energy produced by all trains is $r_t = \sum_{n=1}^{N} r_t^n$.

Suppose now that a track-based electric energy storage is available to collect energy from regenerative braking and re-distribute it to the vehicles in subsequent time steps $t' > t$. Managing a storage

asset requires defining an operating policy to charge/discharge it. Although storage operating policies are usually defined as a function of electricity prices to maximize profit, our goal is to smooth power peaks. We present our policy in Algorithm 2, where $e_0 := (\gamma_1 + \gamma_2 v_{\text{CRUISE}} + \gamma_3 v_{\text{CRUISE}}^2) \cdot v_{\text{CRUISE}} \Delta t$ denotes the baseline energy consumption (kWh) of a train running at constant cruising speed during a time interval.

**Algorithm 2:** Storage operation

**Input:** Energy consumption $e_t^n$ for $t \in \mathcal{T}$ and $n = 1, \dots, N$ from (4); Storage level $L \leftarrow 0$; Baseline energy $e_0$; $\mu \geqslant 0$

**for** $t = 1, \dots, T$ **do**
- Compute regenerative energy $r^t = \sum_{n=1}^{N} |\min\{e_t^n, 0\}|$
- Charge storage $L \leftarrow L + r_t$
- **for** $n = 1, \dots, N$ **do**
  - **if** $L > 0 \ \wedge \ e_n^t > \mu e_0$ **then**
    - Update consumption $e_n^{t,*} \leftarrow \max\{\mu e_0, e_n^t - L\}$
    - Discharge storage $L \leftarrow L - (e_n^t - e^{t,*})$

**Output:** New consumption $e_t^{n,*}$ for $t \in \mathcal{T}, n = 1, \dots, N$

The intuition behind Algorithm 2 is that at least some trains will consume more energy than $e_0$ during a power peak. Thus, the available regenerative energy, tracked by $L$, compensates for the excess of energy with respect to a quantity $\mu e_0$. Regenerative energy not used in the current period charges the storage. The parameter $\mu$ encodes how conservative the policy is. Setting high values of $\mu$ results in the storage providing energy only during high peaks, and increases the chance of not using some regenerative energy before the end of the simulation horizon $T$. Vice versa, with low $\mu$ values the storage more easily supplies electricity, at the risk that this electricity does not go towards shaving the peak points. Although for simplicity we assume here the storage has perfect efficiency and enough capacity to store all energy produced by braking, note that Algorithm 2 can be easily tweaked to account for any round-trip efficiency value and a maximum storage capacity (see De La Torre et al. 2014 for a study on optimal sizing of energy storage in railways). Onboard (i.e., moving) storage systems may also be considered, but in this case a policy to allocate regenerative energy across multiple onboard storage units needs to be defined as well.

We eventually consider a train control measure that does not rely on assumptions on the electric rail system technology. To better spread over time the re-acceleration periods of different trains after a yellow signal is triggered, we consider a *fixed waiting time* rule. More precisely, after a vehicle decelerates and reaches the given approach speed $v_{\text{APPROACH}}$, it must wait for a predetermined amount of time ($\delta$ seconds) before being allowed to re-accelerate. Due to the safety system, more downstream trains may have to reach speeds lower than $v_{\text{APPROACH}}$, or even stop, to respect the

headway constraints. In this case, the fixed waiting time applies to the lowest speed reached.

# 4. Results and discussion

## 4.1 Parameters and computational setup

We start by briefly introducing the computational setting. The simulation parameters employed are summarized in Table 1 and largely follow Corman et al. (2021) for the stochastic process models and Trivella et al. (2021) for the train parameters (e.g., resistance parameters). We consider a system of $N = 6$ consecutive trains, which may occur in high capacity corridors. We assume trains are identical, i.e., they are subject to the same dynamics. To estimate the KPIs described in Section 3.2, we simulated 5000 trajectories of this system for a time horizon $T = 2000$s discretized with $\Delta t = 1$s. In this setting, the total computation time for the simulation was roughly 40 and 72 seconds for the OU and DMR model, respectively, when using Matlab R2021b on a laptop with a processor i7-10610U and 16 GB RAM.

Table 1: Parameters of trains and processes.

| Name | Value | Unit | Name | Value | Unit |
|---|---|---|---|---|---|
| $m$ | 500 | t | $v_{\text{CRUISE}}$ | 35 | m/s |
| $\rho$ | 1.06 | - | $v_{\text{MAX}}$ | 40 | m/s |
| $\gamma_1$ | 5.8 | kN | $v_{\text{APPROACH}}$ | 20 | m/s |
| $\gamma_2$ | 0.072 | kN s/m | $a_{\text{DET}}$ | $-0.55$ | m/s |
| $\gamma_3$ | 0.013 | kN $(\text{s/m})^2$ | $\theta_1$ | 1.05 | - |
| $\alpha_n$ | $2 \cdot 10^{-5}$ | - | $\theta_2$ | 1 | - |
| $\beta_n$ | 0.02 | - | $\lambda_1$ | 2 | - |
| $\sigma_n$ | 0.05 | - | $\lambda_2$ | 1 | - |
| $d_0$ | 3.2 | km | $w$ | 1 | - |
| $d_{\text{MIN}}$ | 3.0 | km | $\eta$ | 0.7 | - |

We consider two specifications of the deterministic model, named $\text{DET}_0$ and $\text{DET}_+$, at varying initial conditions. $\text{DET}_0$ is such that $\bar{v}_n = 35$ m/s for all trains, whereas for $\text{DET}_+$ we set $\bar{v}_1 = 35$ m/s and $\bar{v}_n = 36$ m/s for $n = 2, \dots, 6$ (see the related discussion in Section 3.1). For these models, the computational time to estimate the KPIs is negligible as one trajectory is sufficient to fully characterize the system.

We present our results and insights next. Sections 4.2 and 4.3 do not make use of the peak reduction strategies, whose effect is investigated later in Sections 4.4 and 4.5.

## 4.2 Analysis of a trigger event

In this section, we use the OU energy profile displayed in the middle panel of Figure 1 to better illustrate the propagation of an individual yellow signal event. The peak in this profile is due to four trains accelerating in a short time frame as shown in the time-speed profiles in Figure 2. Note that

we varied the scale of the y-axis in the top and bottom panels to clearly distinguish the stochastic speed variations (mostly occurring within a band of $\pm 0.5$ m/s) from the yellow signal effect.

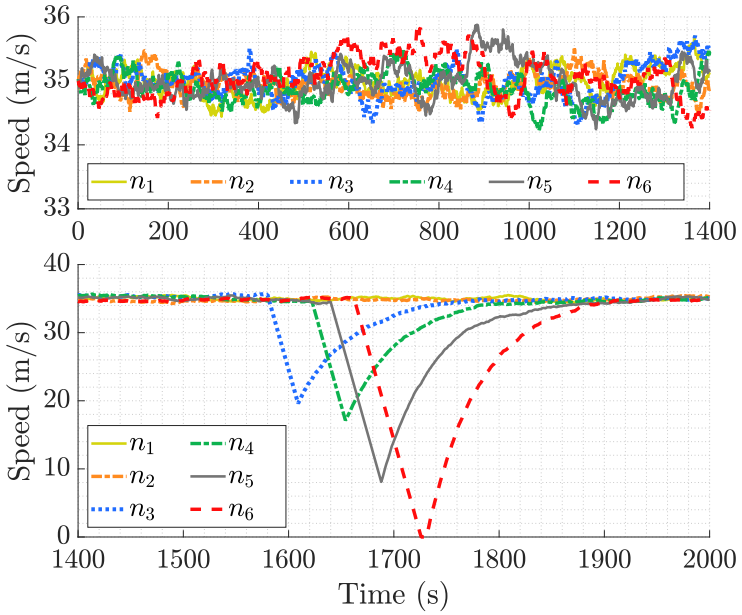


Figure 2: Time-speed profiles of six trains in one trajectory.

Train 3 is the first to trigger a yellow signal and decelerate, which causes train 4 to decelerate too, followed by trains 5 and 6. Interestingly, whilst the first affected train decelerates to $v_{\text{APPROACH}} = 20$ m/s before re-accelerating, the downstream vehicles may have to reach lower speeds, and potentially even stop, before the headway is restored and they can accelerate again. This implies that the traffic regularity is more sensitive to yellow signals when more consecutive trains are running.

To visualize the same effect from another angle, we show in Figure 3 the space lost by the different trains compared to a baseline with constant speed $v_{\text{CRUISE}}$. As before, downstream vehicles are disproportionately affected by a triggered yellow signal. In this example, the span between first

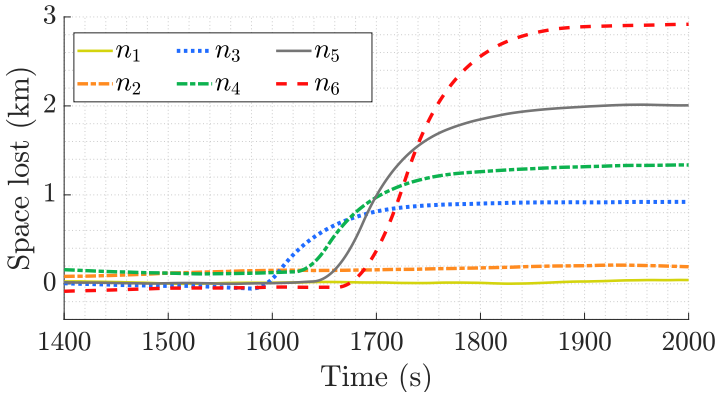


Figure 3: Space lost with respect to a deterministic speed baseline.

and last simulated vehicle increases by roughly 3 km during the event.

We also present a heatmap of train accelerations in Figure 4. The different shades of orange correspond to the background variations due to the stochastic process, whereas deceleration and acceleration phases caused by the triggering of a yellow signal are clearly visible by the darker and lighter colors, respectively. By overlaying this heatmap with the trajectories in Figure 2, we notice that the peak point occurs at 1700–1800 seconds, corresponding to the period in which most trains are indeed accelerating, thus requiring a large joint traction force.

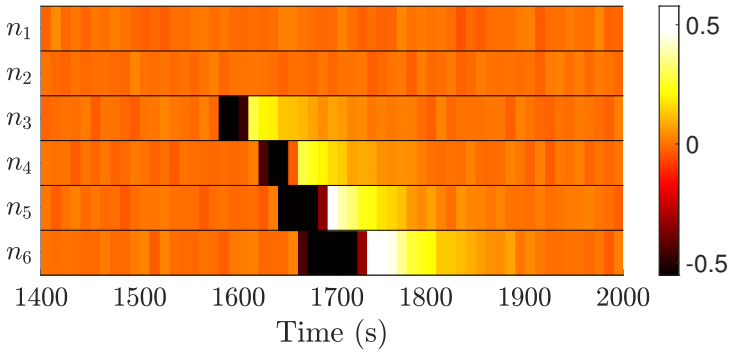


Figure 4: Synchronization of acceleration and deceleration activities.

### 4.3 Analysis of key performance indicators

We analyze the aggregate performance of the system from a traffic regularity perspective in Tables 2–3 for both stochastic models (OU, DMR) and deterministic models ($\text{DET}_0$, $\text{DET}_+$).

Table 2: Traffic regularity KPIs.

| | | Train (1 is the leader) | | | | | |
|---|---|---|---|---|---|---|---|
| KPI | Model | 1 | 2 | 3 | 4 | 5 | 6 |
| K1 (% triggers) | OU | 0 | 15.2 | 29.0 | 41.7 | 52.0 | 60.1 |
| | DMR | 0 | 2.8 | 4.7 | 6.0 | 7.6 | 8.7 |
| | $\text{DET}_0$ | 0 | 0 | 0 | 0 | 0 | 0 |
| | $\text{DET}_+$ | 0 | 100 | 100 | 100 | 100 | 100 |
| K2 (FTTY (s)) | OU | - | 1891 | 1795 | 1702 | 1625 | 1560 |
| | DMR | - | 1981 | 1970 | 1961 | 1950 | 1944 |
| | $\text{DET}_0$ | - | >2000 | >2000 | >2000 | >2000 | >2000 |
| | $\text{DET}_+$ | - | 201 | 228 | 255 | 282 | 309 |

Table 3: Throughput of the corridor.

| KPI | OU | DMR | $\text{DET}_0$ | $\text{DET}_+$ |
|---|---|---|---|---|
| K3 (vehicles/hour) | 35.4 | 38.9 | 39.4 | 27.0 |

We observe the following important points:

- The OU model incurs many more triggers than the DMR model (see K1), and when this happens, it is earlier for any of the followers as shown by the FTTY indicator K2. These results suggest that an ATO model aware of the location of the traffic ahead leads to a higher level of traffic regularity that enables to better exploit the capacity of the corridor. This is confirmed by an almost 10% higher throughput in DMR compared to OU (see K3).
- The percentage of yellow signals increases substantially when moving from the first follower (train 2) to the last (train 6). This implies that it is common for yellow signals to propagate backwards, that is, a train $n$ decelerating will very likely trigger train $n+1$ to decelerate or brake too. This is a major cause of peaks in energy consumption.
- Deterministic strategies showcase two extreme behaviors: $\text{DET}_0$ is the unrealistic situation of perfect operations, where no yellow signal occurs, whereas in $\text{DET}_+$ all followers triggers a yellow signal due to their higher speed compared to the first leader (although by just 1 m/s).

Next, we now focus on the energy properties of the six-train system and report in Table 4 the related KPIs. Recall that K4, K5, and K6 represent the average total consumption, average maximum consumption, and percentage of energy profiles with a detected peak, respectively (see Section 3.2 for details).

Table 4: Energy related KPIs.

| KPI | OU | DMR | $\text{DET}_0$ | $\text{DET}_+$ |
|---|---|---|---|---|
| K4 (kWh) | 2876 | 2814 | 2800 | 3312 |
| K5 (kWh/30s) | 64.7 | 52.0 | 42.4 | 83.9 |
| K6 (%) | 59.1 | 9.3 | 0 | 100 |

What we observe from the table is the following:

- [K4]: The energy consumption under OU is 2.2% higher than DMR. Indeed trains under DMR less frequently have to decelerate, brake, and accelerate following a yellow signal. This difference translates to a substantial saving of energy and costs with an ATO-based system, especially when considering the consumption of an entire railway network for a year. Compared to the ideal situation represented by $\text{DET}_0$, the total consumption with DMR is only 0.5% higher, while with OU is 2.7% higher. The consumption under $\text{DET}_+$ is very large because this deterministic profile includes a yellow signal with certainty.
- [K5]: OU energy profiles exhibit a highest consumption point that is on average 25% higher than that of DMR profiles, which is a significant difference. Notice that this KPI averages all

profiles with and without detected peaks and that an individual peak can exceed 80 kWh/30s. The two deterministic models display extreme behaviors: $\mathrm{DET}_0$ has a constant, low energy consumption over the horizon, while $\mathrm{DET}_+$ has a peak of about 84 kWh/30s.

- [K6]: Our method detected peaks in about 60% of the OU profiles, while the same number is less than 10% for DMR. Naturally, the estimates of this KPI are quite related to those of K1 for the last follower.

The main implication from these results is that an ATO system (represented here by the DMR process) has the potential to not only reduce the overall energy requirements but also to prevent the occurrence of critical peaks in consumption.

What we discussed is also evident from Figure 5, showing the first 50 energy profiles for OU (top panel) and DMR (middle panel). We plot the deterministic $\mathrm{DET}_+$ profile too (bottom panel), and the fixed baseline consumption of $\mathrm{DET}_0$.

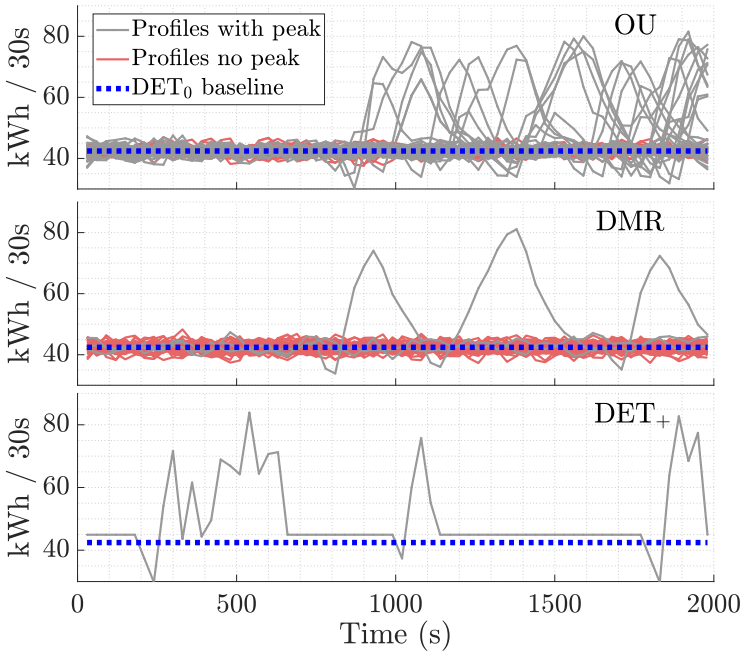


Figure 5: Simulated energy profiles for model OU, DMR, and $\mathrm{DET}_+$.

While a considerable number of OU profiles include at least one peak (32/50), only a few DMR profiles do (3/50). In our setting, the peaks often reach double the regular energy consumption level (i.e., with no train affected by a yellow signal), and mostly appear in the second part of the horizon as the initial state of the system fulfills the minimum safety distance. We investigate next the usefulness of peak reduction strategies.

### 4.4 Analysis of peak reduction strategies

We focus hereafter on the OU process, as this is the stochastic model that could benefit most from fewer peaks and smaller peak size. In Figure 6, we illustrate the effect of peak reduction strategies on the two energy profiles already shown in the middle and bottom panels of Figure 1. Specifically, we consider the fixed waiting time rules at varying $\delta$ (labeled "Fixed"), and the use of regenerative braking, with storage ("Reg+Stor") and without it ("Reg"), assuming $\eta = 0.7$ (we tested different values too but our key findings do not change). We use $\mu = 1$ when managing the storage (see Algorithm 2) and analyze different values of this parameters later in this section.

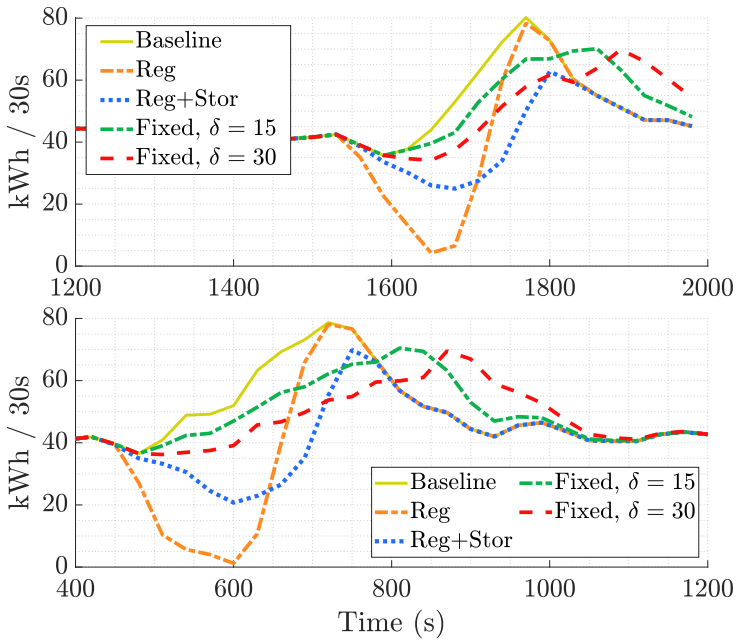


Figure 6: Energy profiles under different peak reduction strategies.

Each strategy has a different effect on the original profile (continuous line). Regenerative energy alone reduces the overall consumption but does not smooth the peak in its highest point. When storage is available, however, the resulting peak is much smaller. The effect of fixed waiting strategies is different as the peak is both reduced in size and spread over time, while it is unclear if the total consumption decreases in these cases.

To better understand the aforementioned changes, Figure 7 illustrates the speed trajectories of the six trains associated with the energy profile in the top panel (which was the same example also considered in Section 4.2). Recall that the use of regenerative braking, with and without storage, does not alter the speed trajectories, whereas fixed waiting rules affect the train dynamics as well. This is why we do not show the speed trajectories under regenerative energy: they coincide with the baseline trajectories in the top panel of Figure 7 ($\delta = 0$). From this figure, it is evident that the higher is the waiting time $\delta$, the more the trains are spread apart from each other after a yellow

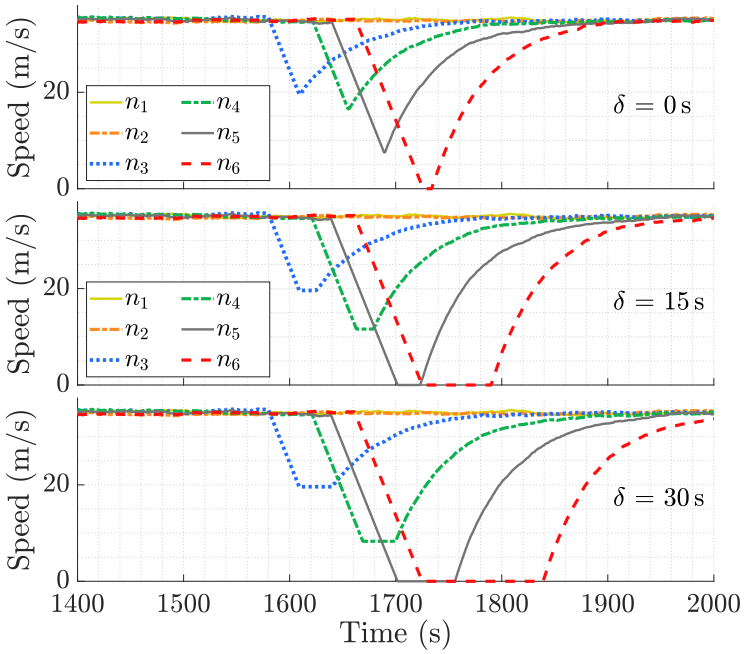


Figure 7: Speed trajectories during a trigger event at varying waiting time $\delta$.

signal, and with that the acceleration activities. Moreover, the more downstream trains may have to wait longer than $\delta$ before the headway is restored and they can re-accelerate. Thus, although fixed waiting rules can help in shaving power peaks, they may also slow the traffic down and affect the throughput of the system, as we examine next.

In Table 5, we report a subset of the KPIs for a system using regenerative braking, fixed waiting rules, and a combination of them. The main findings from these results are the following:

- [K3]: The throughput decreases, approximately linearly, when the fixed waiting time $\delta$ in-

Table 5: KPIs of the system under different peak reduction strategies.

| | | Fixed waiting time $\delta$ (s) | | | | | | |
|---|---|---|---|---|---|---|---|---|
| Technology | KPI | 0 | 10 | 20 | 30 | 40 | 50 | 60 |
| - | K3 | 35.4 | 34.0 | 33.0 | 31.7 | 30.6 | 30.1 | 29.3 |
| | K4 | 2876 | 2877 | 2870 | 2864 | 2856 | 2845 | 2837 |
| | K5 | 64.7 | 63.6 | 62.2 | 61.6 | 60.6 | 59.7 | 59.2 |
| Reg | K3 | 35.4 | 34.0 | 33.0 | 31.7 | 30.6 | 30.1 | 29.3 |
| | K4 | 2781 | 2773 | 2768 | 2761 | 2757 | 2753 | 2748 |
| | K5 | 64.4 | 63.3 | 62.0 | 61.4 | 60.5 | 59.6 | 59.2 |
| Reg+Stor ($\mu = 1$) | K3 | 35.4 | 34.0 | 33.0 | 31.7 | 30.6 | 30.1 | 29.3 |
| | K4 | 2795 | 2788 | 2780 | 2775 | 2769 | 2765 | 2763 |
| | K5 | 59.3 | 59.5 | 59.1 | 58.6 | 58.1 | 57.7 | 57.4 |

creases. In particular, this KPI goes from 35.4 to 29.3 vehicles/hour when $\delta$ varies from 0 to 60 seconds, which is a 17% reduction.

- [K4]: The total energy consumption is reduced only marginally by variations of $\delta$. However, exploiting regenerative braking brings savings of 3.3% on average.

- [K5]: The highest consumption point decreases by 8.5% on average when $\delta$ increases from 0 to 60 seconds. When restricting to energy profiles with detected peaks, this improvement exceeds 10%, which is substantial. Regenerative braking alone does not help much in shaving the peak, while it is very effective when it is coupled with an electricity storage, with an improvement of 8.5%.

Beside $\delta$, another important tunable parameters is $\mu$, which defines the storage operating policy. Thus, we examine how the KPIs change when using regenerative braking with storage at varying $\mu$. Figure 8 shows an energy profile under values of $\mu$ from 0.6 to 2.2. Increasing $\mu$ is beneficial to smooth the peak and, for instance, the highest point in this profile decreases from 71 to 50 kWh when $\mu$ goes from 0.6 to 1.8. However, increasing $\mu$ from 1.8 to 2.2 results in a higher peak of 54.5 kWh, and a higher energy consumption too as it can be seen from the area under the profiles. In fact, $\mu$ represents a threshold for the storage to be discharged and setting too high values of it may result in very conservative policies.

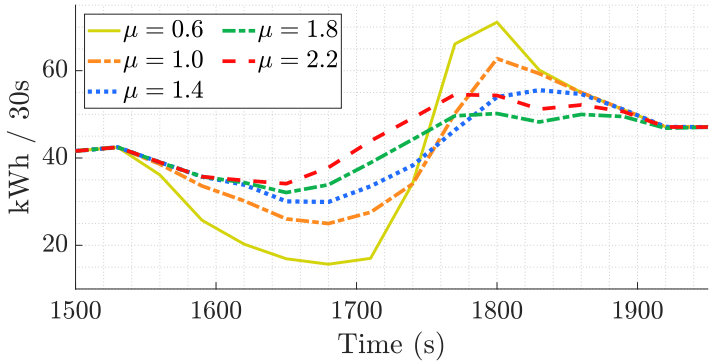


Figure 8: Energy profile with regenerative braking and storage at varying $\mu$.

Table 6 reports estimates of the energy KPIs for operating strategies at varying $\mu$ (notice that the traffic KPIs K1–K3 do not change with $\mu$; hence, they are not included in this table). The energy consumption (K4) indeed increases with $\mu$ but only marginally. However, the percentage of trajectories with a peak (K6) varies from 31.6% to 51.4% when $\mu$ is increased from 1.6 to 2.2, which is a substantial increase indicating that the behavior of K6 is not monotone in $\mu$. The same holds for K5 (average peak), which shows a small increment after $\mu = 2$. Overall, the value $\mu = 1.6$ achieves the best trade-off for the considered experimental setup.

Table 6: Policy performance at varying storage threshold multiplier $\mu$.

| KPI | 0.6 | 0.8 | 1.0 | 1.2 | 1.4 | 1.6 | 1.8 | 2.0 | 2.2 |
|---|---|---|---|---|---|---|---|---|---|
| K4 | 2784 | 2790 | 2796 | 2799 | 2800 | 2802 | 2806 | 2813 | 2819 |
| K5 | 62.5 | 61.2 | 59.3 | 57.1 | 55.2 | 53 | 52.1 | 52.7 | 53.4 |
| K6 | 52.2 | 51.1 | 49.4 | 45.5 | 39.9 | 31.6 | 36.3 | 46.4 | 51.4 |

### 4.5 Trade-offs between objectives

The findings in Sections 4.3–4.4 have underscored several conflicts that exist among different objectives, especially between the traffic-related and the energy-related KPIs. Therefore, we investigate more systematically some of the trade-offs that arise under different peak reduction strategies.

Figure 9 illustrates 4 trade-offs under 4 strategies. Recall that "Reg", "Stor", and "Fixed" in the name denote, respectively, the use of regenerative energy, storage, and fixed waiting rules. Strategies with "Fixed" are studied for varying $\delta \in [0, 60]$, while "Reg+Stor" for varying $\mu \in [0.6, 2.2]$. "Fixed+Reg+Stor" uses $\mu = 1.6$. To help identifying the best solutions, in each subplot we have

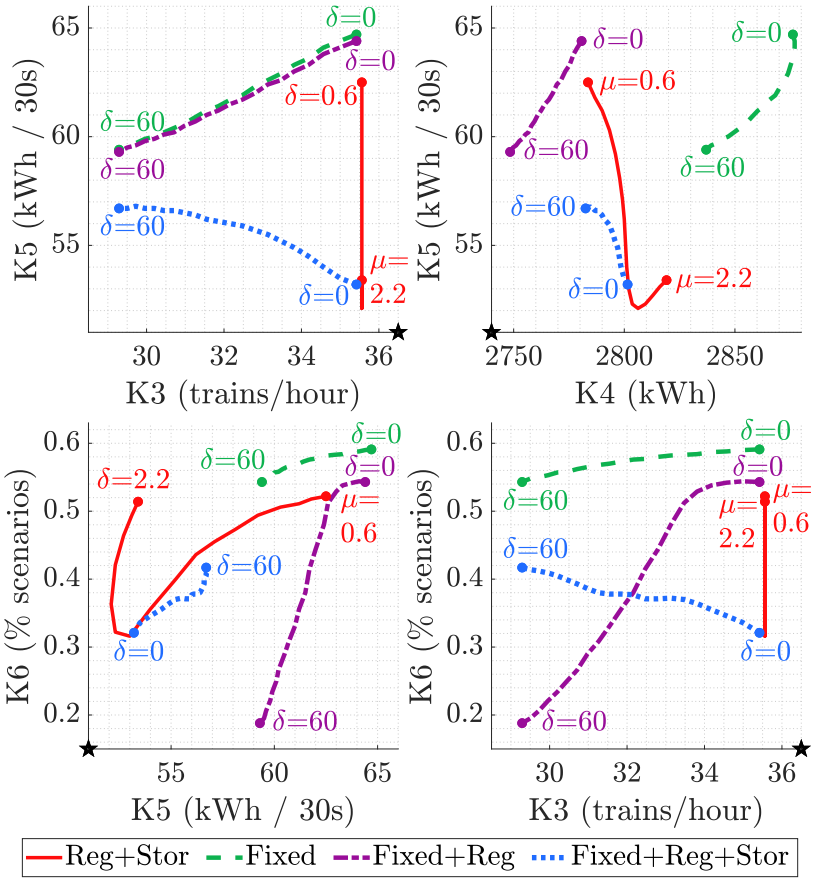


Figure 9: Trade-off between KPIs under different peak reduction measures.

marked with a star the improving direction of the trade-off. In other words, we prefer solutions that are as close as possible to the marked corner.

Drawing conclusions about these results is non-trivial as no strategy dominates the others in managing all KPIs. Fixed waiting rules behave quite differently depending on whether regenerative braking and storage are used. In general, coupling regenerative braking and a well tuned storage operating policy, i.e., with $\mu = 1.6$, seems to work well in most cases. However, deviating from this value of $\mu$ always worsens at least one KPI. Similarly, the effect of varying $\delta$ in the other strategies is mixed and never improves all KPIs jointly. The main takeaway from this analysis is that practical approaches to reduce power peaks in busy railway corridors should be designed carefully and tested across multiple dimensions, limiting the risk that improving one KPI negatively affects several others.

## 5. Conclusion

This work is the first to analyze a stochastic railway traffic flow model for a string of leader-follower trains. By simulating different stochastic processes, we observed that the propagation of yellow signals in such a system and the consequent synchronized acceleration of trains may generate significant peaks in energy use, which is a main concern in the modern railway industry due to high energy prices and environmental concerns.

We thus proposed peak reduction measures that rely on technological assumptions (regenerative braking, energy storage) and/or train control (fixed waiting rules). In an extensive numerical study, we examined the performance of the dynamic system in terms of traffic regularity and energy consumption. We provided insights on the potential benefits of ATO for both smoothing peaks and improving regularity, and on the effectiveness of different peak reduction measures, potentially combined. We finally quantified and discussed the trade-offs that arise between KPIs (e.g., energy vs traffic regularity).

Future research directions include developing alternative peak reduction strategies, for example, based on mathematical programming models to coordinately control vehicles when a yellow signal has been triggered. Embedding such strategies in our simulation framework may be computationally challenging though. Another avenue would be calibrating the parameters of the stochastic processes based on real data. At the time of writing, a comprehensive dataset to allow for such calibration is not available to the authors, and these parameters are defined based on the railway literature and simulation experiments. Finally, additional sensitivity analysis may be conducted on other parameters, such as the initial headway between trains, examining how this relates to the common target of achieving a 80% of capacity utilization (see UIC Code, Norm 406).

## Acknowledgments

The second author was supported by the Swiss National Science Foundation under Project 1481210/-DADA. This paper builds on an extended abstract that was accepted for presentation at the 10th Symposium of the European Association for Research in Transportation (hEART 2022; Trivella and Corman 2022)

## References

A. Albrecht, P. Howlett, P. Pudney, X. Vu, and P. Zhou. The key principles of optimal train control—part 1: Formulation of the model, strategies of optimal type, evolutionary lines, location of optimal switching points. *Transportation Research Part B: Methodological*, 94:482–508, 2016. ISSN 0191-2615.

T. Albrecht. Reducing power peaks and energy consumption in rail transit systems by simultaneous train running time control. *WIT Transactions on State-of-the-art in Science and Engineering*, 39, 2010.

A. Bärmann, A. Martin, and O. Schneider. A comparison of performance metrics for balancing the power consumption of trains in a railway network by slight timetable adaptation. *Public Transport*, 9:95–113, 2017.

S. Binder, Y. Maknoon, and M. Bierlaire. The multi-objective railway timetable rescheduling problem. *Transportation Research Part C: Emerging Technologies*, 78:78–94, 2017.

V. Cacchiani and P. Toth. Robust train timetabling. In *Handbook of Optimization in the Railway Industry*, pages 93–115. Springer, 2018.

A. Caprara, M. Fischetti, and P. Toth. Modeling and solving the train timetabling problem. *Operations Research*, 50(5):851–861, 2002.

F. Corman, A. Trivella, and M. Keyvan-Ekbatani. Stochastic process in railway traffic flow: Models, methods and implications. *Transportation Research Part C: Emerging Technologies*, 128:103167, 2021.

S. De La Torre, A. J. Sánchez-Racero, J. A. Aguado, M. Reyes, and O. Martínez. Optimal sizing of energy storage for regenerative braking in electric railway systems. *IEEE Transactions on Power Systems*, 30 (3):1492–1500, 2014.

V. De Martinis and F. Corman. Data-driven perspectives for energy efficient operations in railway systems: Current practices and future opportunities. *Transportation Research Part C: Emerging Technologies*, 95:679–697, 2018.

EU. European Union - 2030 Climate Target Plan, 2021. URL https://ec.europa.eu/clima/eu-action/european-green-deal/2030-climate-target-plan_en. Accessed 9 May 2022.

A. González-Gil, R. Palacin, and P. Batty. Sustainable urban rail systems: Strategies and technologies for optimal management of regenerative braking energy. *Energy Conversion and Management*, 75:374–388, 2013.

I. Hansen and J. Pachl. *Railway timetabling and operations: Analysis, modelling, optimisation, simulation, performance, evaluation*. Eurail press, Hamburg, 2014.

P. Howlett. The optimal control of a train. *Annals of Operations Research*, 98(1):65–87, 2000.

M. Jusup, A. Trivella, and F. Corman. A review of real-time railway and metro rescheduling models using learning algorithms. In *30th International Joint Conference on Artificial Intelligence (IJCAI-21)*, 2021.

M. Khodaparastan, A. A. Mohamed, and W. Brandauer. Recuperation of regenerative braking energy in electric rail transit systems. *IEEE Transactions on Intelligent Transportation Systems*, 20(8):2831–2847, 2019.

S. Lu, P. Weston, S. Hillmansen, H. B. Gooi, and C. Roberts. Increasing the regenerative braking energy for railway vehicles. *IEEE Transactions on Intelligent Transportation Systems*, 15(6):2506–2515, 2014.

OWiD. Our World in Data - Emissions by sector, 2016. URL https://ourworldindata.org/emissions-by-sector. Accessed 9 May 2022.

Y. Qin, X. Hu, Z. He, and S. Li. Longitudinal emissions evaluation of mixed (cooperative) adaptive cruise control traffic flow and its relationship with stability. *Journal of the Air & Waste Management Association*, 70(7):670–686, 2020.

Railenergy. Innovative integrated energy efficiency solutions for railway rolling stock, rail infrastructure and train operation, 2016. URL http://www.railenergy.org/background.shtml. Accessed 9 May 2022.

X.-C. Ran, S.-K. Chen, G.-H. Liu, and Y. Bai. Energy-efficient approach combining train speed profile and timetable optimisations for metro operations. *IET Intelligent Transport Systems*, 14(14):1967–1977, 2020.

D. Regueiro Sánchez. Quantification and reduction of power peaks in railway networks: a simulation-based approach. Master's thesis, 2021. ETH Zurich.

G. M. Scheepmaker, R. M. Goverde, and L. G. Kroon. Review of energy-efficient train control and timetabling. *European Journal of Operational Research*, 257(2):355–376, 2017.

A. Trivella and F. Corman. Modeling uncertainty dynamics in public transport optimization. In *19th Swiss Transport Research Conference (STRC 2019)*. STRC, 2019.

A. Trivella and F. Corman. An analysis of power peaks in stochastic models of railway traffic. In *hEART 2022 - 10th Symposium of the European Association for Research in Transportation*, 2022.

A. Trivella, P. Wang, and F. Corman. The impact of wind on energy-efficient train control. *EURO Journal on Transportation and Logistics*, 10:100013, 2021.

UIC. International union of railways - Energy efficiency and CO2 emissions, 2017. URL https://uic.org/sustainable-development/energy-and-co2-emissions/. Accessed 21 January 2022.

M. Wang, H. Li, J. Gao, Z. Huang, B. Li, and B. Van Arem. String stability of heterogeneous platoons with non-connected automated vehicles. In *2017 IEEE 20th International Conference on Intelligent Transportation Systems (ITSC)*, pages 1–8. IEEE, 2017.

P. Wang, A. Trivella, R. M. Goverde, and F. Corman. Train trajectory optimization for improved on-time arrival under parametric uncertainty. *Transportation Research Part C: Emerging Technologies*, 119: 102680, 2020.

P. Wang, N. Bešinović, R. M. Goverde, and F. Corman. Improving the utilization of regenerative energy and shaving power peaks by railway timetable adjustment. *IEEE Transactions on Intelligent Transportation Systems*, 2022.

X. Yang, X. Li, B. Ning, and T. Tang. A survey on energy-efficient train operation for urban rail transit. *IEEE Transactions on Intelligent Transportation Systems*, 17(1):2–13, 2015.

X. Yang, A. Chen, B. Ning, and T. Tang. A stochastic model for the integrated optimization on metro timetable and speed profile with uncertain train mass. *Transportation Research Part B: Methodological*, 91:424–445, 2016.

H. Ye and R. Liu. Nonlinear programming methods based on closed-form expressions for optimal train control. *Transportation Research Part C: Emerging Technologies*, 82:102–123, 2017.

J. Yin, T. Tang, L. Yang, Z. Gao, and B. Ran. Energy-efficient metro train rescheduling with uncertain time-variant passenger demands: An approximate dynamic programming approach. *Transportation Research Part B: Methodological*, 91:178–210, 2016.

Y. Zhang, Y. Bai, J. Hu, and M. Wang. Control design, stability analysis, and traffic flow implications for cooperative adaptive cruise control systems with compensation of communication delay. *Transportation Research Record*, 2674(8):638–652, 2020.